



HAL
open science

Fictitious domain method for acoustic waves through a granular suspension of movable rigid spheres

David Imbert, Sean Mcnamara, Yves Le Gonidec

► **To cite this version:**

David Imbert, Sean Mcnamara, Yves Le Gonidec. Fictitious domain method for acoustic waves through a granular suspension of movable rigid spheres. *Journal of Computational Physics*, 2015, 280, pp.676-691. 10.1016/j.jcp.2014.10.006 . insu-01100866

HAL Id: insu-01100866

<https://insu.hal.science/insu-01100866>

Submitted on 7 Jan 2015

HAL is a multi-disciplinary open access archive for the deposit and dissemination of scientific research documents, whether they are published or not. The documents may come from teaching and research institutions in France or abroad, or from public or private research centers.

L'archive ouverte pluridisciplinaire **HAL**, est destinée au dépôt et à la diffusion de documents scientifiques de niveau recherche, publiés ou non, émanant des établissements d'enseignement et de recherche français ou étrangers, des laboratoires publics ou privés.

Fictitious domain method for acoustic waves through a granular suspension of movable rigid spheres

D. Imbert^{a,c,1}, S. McNamara^{a,c,*}, Y. Le Gonidec^{b,c}

^a*Institut de Physique de Rennes (UMR Université de Rennes 1 / CNRS 6251)*

^b*Géosciences Rennes (UMR Université de Rennes 1 / CNRS 6118)*

^c*Campus de Beaulieu, 263 av. du Général Leclerc, CS 74205, 35042 RENNES CEDEX, FRANCE*

Abstract

We develop a model to couple acoustic waves and the motion of rigid movable grains in a submerged suspension. To do so, we use the fictitious domain method based on distributed Lagrange multipliers to enforce the natural jump condition of the wave equation and a rigidity constraint. One can then model the granular medium with "Molecular Dynamics" or related methods. Both dynamic and acoustic numerical results are compared with analytic solutions of acoustics and an estimation of the error is given. We show energy transfers between two submerged grains separated by water and linked to their own spring while oscillating. The model is applied at large scale with a suspension of many grains to foresee its future possibilities.

Keywords: granular medium, suspension, fictitious domain method, distributed Lagrange multipliers, movable rigid grains, acoustic wave equation

1. Introduction

In marine Geosciences, acoustic probing is commonly used to detect subsurface reflectors, characterize their physical properties and study geophysical processes such as slope instabilities. In particular, undersea sediment layers constitute granular materials which pore space is filled with water, i. e. grains are movable bodies. Such layers are acoustically complex materials where sound waves can be multi-scattered and reflected at fluid-grain interfaces. Experiments with model spherical grains under water have been performed to better understand the acoustic behavior of granular media in equilibrium [1] or tilted under gravity [2, 3]. These experiments clearly highlight the contribution of the fluid-grain interaction on the acoustic measurements, which can also be affected by inter-particle contacts [4].

In the case of pores filled with air, dry granular materials are commonly modeled using discrete element methods such as "Molecular Dynamics" [5, 6]. Each grain is represented using a rigid and

[☆]This work was supported by the ANR project STABINGRAM No. 2010-BLAN-0927-01.

^{*}Corresponding author.

Email addresses: david.imbert.1@free.fr (D. Imbert), sean.mcnamara@univ-rennes1.fr (S. McNamara), yves.legonidec@univ-rennes1.fr (Y. Le Gonidec)

¹D. Imbert's work was supported by the grant No. 211-14-231/ARED from the Région Bretagne.

incompressible sphere completely characterized by the position of its center and its radius. The air filling the pores can be neglected because its density is very low, so that the momentum it transmits is negligible. In the case of pores filled with water, the momentum transmitted by the fluid can no longer be neglected. Thus, discrete element methods can not be used to model submerged granular media. Well known numerical models exist to model sound waves in a liquid: for example finite differences [7, 8] or finite elements [9, 8]. But to our knowledge, none of them usually consider neither the coupling between the wave and the motion of grains, nor the inter-particles contacts.

The fictitious domain method based on Lagrange multipliers was introduced in [10] and started to be popular two decades ago when applied to Navier-Stokes equations [11] and then for scattering problems in acoustics [12]. The particularity of this method is to work with two independent finite element meshes: the first one regular and time-independent and the second one unstructured and possibly time-dependent. This last attribute was first applied for forced displacement of particles in [13] and to model vibrations of the membrane of a kettledrum [14]. Introduction of *distributed* Lagrange multipliers [15] allowed simulation of freely movable particles through a *rigid body motion constraint* applied inside particles [16]. The fictitious domain method based on distributed Lagrange multipliers was also developed in [17] for the mixed formulation of the acoustic wave equation with Dirichlet conditions.

In this work, we unite a finite element method to a discrete element model through the fictitious domain method, yielding a single method capable of describing acoustic propagation by both the fluid and inter-granular contacts.

To our knowledge, our model introduced in [18] is the first to couple the acoustic wave equation governing the fluid to the dynamic equations governing the motion of rigid movable grain. However, in that work, we simulated a single rigid sphere in a sound wave, and we compared only its velocity to the analytic solution. In addition to results on the dynamic of the grain, our model allows each grain to generate its own acoustic field when it is under a force due to another incident wave but also due to any other forces acting on it such as a contact force or the gravity. These resulting acoustic fields have never been validated and confronted to analytic solutions.

In the present paper, we present a major development of the model introduced in [18]. First of all, we take on a new mixed finite elements method based on standard conforming finite elements to fix severe convergence issues of the fictitious domain method. We also change the numerical scheme to improve energy conservation. Finally, the model is now able to work with several grains and we illustrate that with new numerical experiments.

The paper is subdivided into 2 main parts. In section 2 and 3, we are describing the model, i. e. governing equations, the fictitious domain method, and the computational scheme. Section 4 deals with three numerical experiments, involving one, two and many movable grains submerged in water, respectively. With the first experiment, both dynamic and acoustic numerical results are compared with analytic solutions of acoustics and an estimation of the error is given. With the second experiment, we analyse the energy transfers between two oscillating grains separated by water and linked with their own springs. In the last experiment, we highlight the potential of the model to sound a suspension of grains with acoustic pulses.

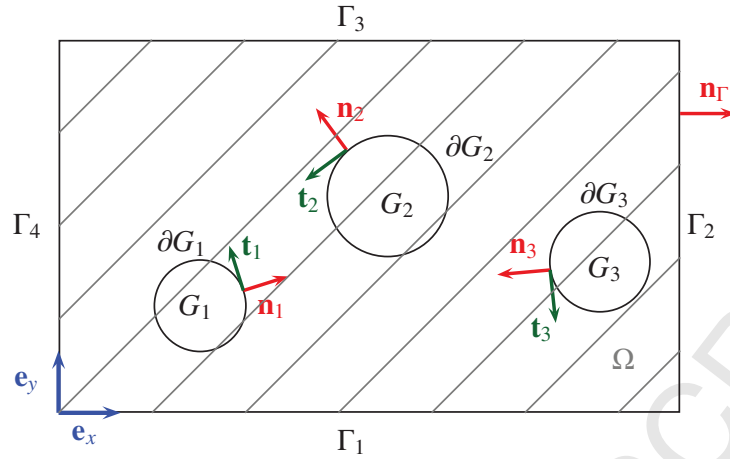


Figure 1: System with the different domains: domains G_k are the domain of each grain k ; and the hatched rectangle is the whole domain Ω and Γ its boundary.

2. Governing equations

A schematic representation of rigid bodies in a fluid matrix is considered on Fig. 1. Let Ω be the domain which includes a set of grains G and a fluid matrix $\Omega \setminus G$. The domain G is subdivided into N_G circular subdomains G_k , one for each grain, such that $G = \cup G_k$. Let Γ be the boundary of the whole domain Ω , ∂G_k the boundary of each domain G_k , and therefore let ∂G be the boundary of the domain G . We also define \mathbf{n}_k the outgoing normal unit vector of the boundary ∂G_k , \mathbf{t}_k the tangential unit vector, and \mathbf{X}_k the position of the center of the subdomain G_k .

We consider that the fluid is perfect, i.e. non viscous, non heat conducting and isentropic. The perfect fluid approximation is commonly used in acoustics because the scattering and transport of energy are much more important than dissipation due to viscosity. Moreover, the variations of the pressure fields are small compared to their mean value and the density of the fluid ρ_0 and the velocity of sound in the fluid c_0 are constant. These assumptions allow use of the mixed formulation of the acoustic wave equation governing the fluid.

2.1. Strong forms

We can write the acoustic wave equation as a system of two equations in terms of pressure field p and velocity field \mathbf{u} :

$$\begin{cases} \rho_0 \frac{\partial \mathbf{u}}{\partial t} + \nabla p = \mathbf{0} & \text{in } \Omega \setminus G & (1a) \\ \frac{1}{\rho_0 c_0^2} \frac{\partial p}{\partial t} + \nabla \cdot \mathbf{u} = 0 & \text{in } \Omega \setminus G & (1b) \end{cases}$$

The second system of equations governs the motion of grains:

$$\rho S_k \frac{d\mathbf{U}_k}{dt} = - \int_{\partial G_k} p \mathbf{n}_k dl + \mathbf{F}_k \quad \forall k = 1, 2, \dots, N_G \quad (2)$$

Here S_k and \mathbf{U}_k are the surface (in a 2D domain) and the velocity of the grain k , respectively. All grains have the same density $\rho_k = \rho \forall k = 1, 2, \dots, N_G$. \mathbf{F}_k can handle any other extra force, for example if the grain is subjected to the gravity, a spring force, or some interaction forces. Contrary to system (1), Eq. (2) is discrete and therefore allows use of discrete elements methods such that the Molecular Dynamics algorithm [5].

Then, to link systems (1) and (2), we add the natural jump condition of the acoustic wave equation for movable rigid bodies:

$$\mathbf{u} \cdot \mathbf{n}_k = \mathbf{U}_k \cdot \mathbf{n}_k \quad \text{on } \partial G_k \forall k = 1, 2, \dots, N_G \quad (3)$$

Eq. (3) is essential to couple the grains velocity \mathbf{U}_k and the acoustic velocity field \mathbf{u} .

Eq. (3) is just the "slip" boundary condition appropriate for the perfect fluid we are considering, applied to the surface of the grains. The particle rotations do not appear because they couple to the fluid only through tangential viscous stresses exerted by the viscosity of the particle surface. Our fluid is inviscid and therefore this coupling is absent.

Note that the jump condition (3) does not prevent particle rotation. In the special case where \mathbf{F}_k includes friction forces between grains, then an additional term including angular velocity should be added to the first member of Eq. (2). But even in this case, rotations of a sphere in a perfect fluid can not generate any sound.

Another natural consequence of Eq. (3) is that only the normal component of the acoustic velocity field is constrained at the interface. Because of the perfect fluid, we have no information on the tangential component of the velocity field. This is consistent with the governing equation Eq. (1) which allows more freedom for the velocity and pressure fields than the Navier-Stokes equation would do.

Two kinds of boundary conditions are set on the outer frontier $\Gamma = \cup \Gamma_j$ of Ω . On one hand, Perfectly Matched Layers (PML) [19] are set on the bottom side Γ_1 and the top side Γ_3 of the domain Ω but we will not focus on that point to keep equations simple. See [20] for details on the construction of the PML based on a coordinate stretching approach for Maxwell's equations and [17] for the acoustic wave equation. These layers end with a Dirichlet condition applied on the pressure field:

$$p = 0 \quad \text{on } \Gamma_1 \cup \Gamma_3 \quad (4)$$

On the other hand, we set periodic boundary conditions on the right side Γ_2 and the left side Γ_4 of the domain Ω

$$p|_{\Gamma_2} = p|_{\Gamma_4} \quad \text{on } \Gamma_2 \cup \Gamma_4 \quad (5)$$

$$\mathbf{u}|_{\Gamma_2} = \mathbf{u}|_{\Gamma_4} \quad \text{on } \Gamma_2 \cup \Gamma_4 \quad (6)$$

In that way, we can easily generate plane waves which are useful when comparing with analytic solutions of acoustics.

2.2. Weak forms

We write now the weak form of Eqs. (1a) and (2) into a single equation with the unknowns $\mathbf{u} \in H(\text{div}, \Omega \setminus G)$, $\mathbf{U}_k \in \mathbb{R}^2 \forall k = 1, \dots, N_G$ and $p \in L^2(\Omega \setminus G)$:

$$\begin{aligned} \int_{\Omega \setminus G} \rho_0 \frac{\partial \mathbf{u}}{\partial t} \cdot \mathbf{v} \, d\mathbf{x} - \int_{\Omega \setminus G} p \nabla \cdot \mathbf{v} \, d\mathbf{x} + \int_{\Gamma} p \mathbf{n}_{\Gamma} \cdot \mathbf{v} \, d\ell - \int_{\partial G} p \mathbf{n} \cdot \mathbf{v} \, d\ell \\ + \sum_k \left[\rho S_k \frac{d\mathbf{U}_k}{dt} \cdot \mathbf{V}_k - \mathbf{F}_k \cdot \mathbf{V}_k + \int_{\partial G_k} p \mathbf{n}_k \cdot \mathbf{V}_k \, d\ell \right] = 0 \end{aligned} \quad (7)$$

Here $\mathbf{v} \in H(\text{div}; \Omega \setminus G)^2$, $\mathbf{V}_k \in \mathbb{R}^2$, and $q \in L^2(\Omega \setminus G)$ are the respective test functions of \mathbf{u} , \mathbf{U}_k , and p . Eq. (7) was called *combined equation of motion* in [21] and it expresses the conservation of the momentum in the whole domain Ω . We note that the integral on ∂G (last term of the 1st line of (7)) and the sum of hydrodynamic forces (last term of the 2nd line of (7)) cancel each other out if and only if we extend Eq. (3) to the test functions and require $\mathbf{v} \cdot \mathbf{n}_k = \mathbf{V}_k \cdot \mathbf{n}_k \forall k = 1, 2, \dots, N_G$. To take this condition into account, we define a new functional space $\tilde{\mathbb{W}}_{\Omega \setminus G}$ that we also called *combined variation space* in reference to the space introduced in [16] for the Navier-Stokes equation:

$$\tilde{\mathbb{W}}_{\Omega \setminus G} = \left\{ (\mathbf{v}, \mathbf{V}_k) \mid \mathbf{v} \in H(\text{div}; \Omega \setminus G), \mathbf{V}_k \in \mathbb{R}^2; \mathbf{v} \cdot \mathbf{n}_k = \mathbf{V}_k \cdot \mathbf{n}_k \text{ on } \partial G_k \forall k = 1, 2, \dots, N_G \right\} \quad (8)$$

Moreover, boundary conditions (4) and (5) make the integral on Γ vanish, and therefore lead to find $(\mathbf{u}, \mathbf{U}_k) \in \tilde{\mathbb{W}}_{\Omega \setminus G}$ and $p \in L^2(\Omega \setminus G)$ such as:

$$\begin{cases} \int_{\Omega \setminus G} \rho_0 \frac{\partial \mathbf{u}}{\partial t} \cdot \mathbf{v} \, d\mathbf{x} - \int_{\Omega \setminus G} p \nabla \cdot \mathbf{v} \, d\mathbf{x} + \sum_k \left[\rho S_k \frac{d\mathbf{U}_k}{dt} \cdot \mathbf{V}_k - \mathbf{F}_k \cdot \mathbf{V}_k \right] = 0 & (9a) \\ \int_{\Omega \setminus G} \frac{1}{\rho_0 c_0^2} \frac{\partial p}{\partial t} q \, d\mathbf{x} + \int_{\Omega \setminus G} \nabla \cdot \mathbf{u} q \, d\mathbf{x} = 0 & (9b) \end{cases}$$

$\forall (\mathbf{v}, \mathbf{V}_k) \in \tilde{\mathbb{W}}_{\Omega \setminus G}$ and $q \in L^2(\Omega \setminus G)$.

2.3. Fictitious domain method formulation

The fictitious domain method consists in extending Eq. (9) defined in the fluid domain $\Omega \setminus G$ to the domain Ω such that the acoustic fields p and \mathbf{u} are also defined in the whole regular domain Ω . To do so, we proceed in three steps :

1. first, we extend the combined equation of motion (9a) to the whole domain Ω ;
2. then, constraints acting on the grain are enforced in a weak sense using Lagrange multipliers;
3. finally, we extend the linearized continuity equation (9b) to the whole domain using the same constraints

2.3.1. Combined equation of motion for the extended domain

First, we follow the method described in [16] to develop an equation analogous to Eq. (9a) valid in the domain G_k . The extension from one grain G_k to the whole domain $G = \bigcup G_k$ is straightforward. However, we start with a different hypothesis from [16] because we use a different boundary condition on the grain, namely Eq. (3).

Let $(\mathbf{X}_k, \mathbf{e}_r, \mathbf{e}_\theta)$ be an orthonormal basis with the center of the grain \mathbf{X}_k as its origin and $\mathbf{e}_r = \mathbf{n}_k$ and $\mathbf{e}_\theta = \mathbf{t}_k$ orthogonal unit vectors. The following development to find an equation for the extended domain G_k is split into two steps: one to find an expression involving the projection of \mathbf{u} on \mathbf{e}_r and another one for the projection of \mathbf{u} on \mathbf{e}_θ .

Firstly Eq. (3) is extended from ∂G_k to G_k :

$$\mathbf{u} \cdot \mathbf{e}_r = \mathbf{U}_k \cdot \mathbf{e}_r \quad \text{in } G_k \quad (10)$$

Let's call u_r the projection of \mathbf{u} on \mathbf{e}_r :

$$u_r = \mathbf{U}_k \cdot \mathbf{e}_r \quad (11)$$

We can derive Eq. (11) with respect to the time and multiply each member by ρ_0 :

$$\rho_0 \frac{\partial u_r}{\partial t} = \rho_0 \frac{d}{dt} (\mathbf{U}_k \cdot \mathbf{e}_r) \quad \text{in } G_k \quad (12)$$

We introduce the combined variation space $\tilde{\mathbb{W}}_{G_k}$, counterpart of the space $\tilde{\mathbb{W}}_{\Omega \setminus G}$ in G_k :

$$\tilde{\mathbb{W}}_{G_k} = \left\{ (\mathbf{v}, \mathbf{V}_k) \mid \mathbf{v} \in H(\text{div}; G_k), \mathbf{V}_k \in \mathbb{R}^2; \mathbf{v} \cdot \mathbf{n}_k = \mathbf{V}_k \cdot \mathbf{n}_k \text{ on } \partial G_k \right\} \quad (13)$$

The weak form of Eq. (12) can be written:

$$\int_{G_k} \rho_0 \frac{\partial u_r}{\partial t} v_r \, d\mathbf{x} = \int_{G_k} \rho_0 \frac{d}{dt} (\mathbf{U}_k \cdot \mathbf{e}_r) V_{k_r} \, d\mathbf{x} \quad (14)$$

Then, knowing that $\mathbf{e}_r = \cos(\theta) \mathbf{e}_x + \sin(\theta) \mathbf{e}_y$:

$$\int_{G_k} \rho_0 \frac{\partial u_r}{\partial t} v_r \, d\mathbf{x} = \rho_0 \int_0^{R_k} dr \int_0^{2\pi} \frac{d}{dt} (U_{k_x} \cos(\theta) + U_{k_y} \sin(\theta)) (V_{k_x} \cos(\theta) + V_{k_y} \sin(\theta)) \, d\theta \quad (15)$$

we compute integrals in the right hand side of (15):

$$\int_{G_k} \rho_0 \frac{\partial u_r}{\partial t} v_r \, d\mathbf{x} = \rho_0 S_k \frac{d\mathbf{U}_k}{dt} \cdot \mathbf{V}_k \, d\mathbf{x} \quad (16)$$

Now, we do the same for the tangential component of the velocity field $u_\theta = \mathbf{u} \cdot \mathbf{t}_k$ (see Fig. 1 for the direction of \mathbf{t}_k). We begin with another natural jump condition of the wave equation derived from the continuity of the pressure through the interface ∂G_k [22]:

$$\rho_0 \frac{\partial}{\partial t} (\mathbf{u} \cdot \mathbf{t}_k) = \nabla p \cdot \mathbf{t}_k \quad \text{on } \partial G_k \quad (17)$$

As described above, we extend Eq. 17 to G_k , multiply by the test function v_θ and we integrate using the gradient theorem on a closed surface so that:

$$\int_{G_k} \rho_0 \frac{\partial u_\theta}{\partial t} v_\theta \, d\mathbf{x} = 0 \quad (18)$$

Injecting Eq. (18) in Eq. (16) leads to:

$$\int_{G_k} \rho_0 \frac{\partial \mathbf{u}}{\partial t} \cdot \mathbf{v} \, d\mathbf{x} = \rho_0 S_k \frac{d\mathbf{U}_k}{dt} \cdot \mathbf{V}_k \, d\mathbf{x} \quad \forall (\mathbf{v}, \mathbf{V}_k) \in \tilde{\mathbb{W}}_{G_k} \quad (19)$$

To go further, we enforce a divergence free constraint of the velocity field inside the grain G_k to prevent propagation of waves through the grain:

$$\nabla \cdot \mathbf{u} = 0 \quad \text{in } G_k \quad (20)$$

The associated constraint $\nabla \cdot \mathbf{v} = 0$ related to Eq. (20) has to be joined to the functional space $\tilde{\mathbb{W}}_{G_k}$ (13):

$$\mathbb{W}_{G_k} = \left\{ (\mathbf{v}, \mathbf{V}_k) \mid \mathbf{v} \in H(\text{div}; G_k), \mathbf{V}_k \in \mathbb{R}^2; \mathbf{v} \cdot \mathbf{n}_k = \mathbf{V}_k \cdot \mathbf{n}_k \text{ on } \partial G_k; \nabla \cdot \mathbf{v} = 0 \text{ in } G_k \right\} \quad (21)$$

In that way, we can add the missing integral to obtain the analog of Eq. (9a) and the problem is now to find $(\mathbf{u}, \mathbf{U}_k) \in \mathbb{W}_{G_k}$ such as:

$$\int_{G_k} \rho_0 \frac{\partial \mathbf{u}}{\partial t} \cdot \mathbf{v} \, d\mathbf{x} - \int_{G_k} p \nabla \cdot \mathbf{v} \, d\mathbf{x} = \rho_0 S_k \frac{d\mathbf{U}_k}{dt} \cdot \mathbf{V}_k \, d\mathbf{x} \quad \forall (\mathbf{v}, \mathbf{V}_k) \in \mathbb{W}_{G_k} \quad (22)$$

Then, performing the symbolic operation "(9a) + \sum_k (22)" yields to the combined equation of motion for the extended domain with solutions $(\mathbf{u}, \mathbf{U}_k) \in \mathbb{W}_\Omega$:

$$\int_\Omega \rho_0 \frac{\partial \mathbf{u}}{\partial t} \cdot \mathbf{v} \, d\mathbf{x} - \int_\Omega p \nabla \cdot \mathbf{v} \, d\mathbf{x} + \sum_k \left[(\rho - \rho_0) S_k \frac{d\mathbf{U}_k}{dt} \cdot \mathbf{V}_k - \mathbf{F}_k \cdot \mathbf{V}_k \right] = 0 \quad \forall (\mathbf{v}, \mathbf{V}_k) \in \mathbb{W}_\Omega \quad (23)$$

with \mathbb{W}_Ω the combined variation space extended to Ω :

$$\mathbb{W}_\Omega = \left\{ (\mathbf{v}, \mathbf{V}_k) \mid \mathbf{v} \in H(\text{div}; \Omega), \mathbf{V}_k \in \mathbb{R}^2; \mathbf{v} \cdot \mathbf{n}_k = \mathbf{V}_k \cdot \mathbf{n}_k \text{ on } \partial G_k; \nabla \cdot \mathbf{v} = 0 \text{ in } G_k \forall k = 1, \dots, N_G \right\} \quad (24)$$

2.3.2. Enforcement of constraints using Lagrange multipliers

In a second phase, the two constraints $\mathbf{v} \cdot \mathbf{n} = \mathbf{V} \cdot \mathbf{n}$ and $\nabla \cdot \mathbf{v} = 0$ have to be extracted from the combined variation space (24) and added explicitly to Eq. (23) with Lagrange multipliers. For each unknown Lagrange multiplier added, an equivalent equation have to be joined to Eq. (23). The jump condition of the wave equation (3) is enforced using boundary Lagrange multipliers $\lambda_{\partial G}$ on ∂G and *distributed Lagrange multipliers* [15] λ_G are used to enforce the divergence free constraint (20) inside G . The problem is to find $\mathbf{u} \in H(\text{div}, \Omega)$, $\mathbf{U}_k \in \mathbb{R}^2$, $\lambda_{\partial G} \in H^{1/2}(\partial G)$, $\lambda_G \in H^1(G)$ such as:

$$\left\{ \begin{aligned} & \int_\Omega \rho_0 \frac{\partial \mathbf{u}}{\partial t} \cdot \mathbf{v} \, d\mathbf{x} - \int_\Omega p \nabla \cdot \mathbf{v} \, d\mathbf{x} + \sum_k \left[(\rho - \rho_0) S_k \frac{d\mathbf{U}_k}{dt} \cdot \mathbf{V}_k - \mathbf{F}_k \cdot \mathbf{V}_k \right] \\ & + \sum_k \left[\int_{\partial G_k} \lambda_{\partial G} (\mathbf{v} \cdot \mathbf{n}_k - \mathbf{V}_k \cdot \mathbf{n}_k) \, d\ell \right] + \int_G \lambda_G \nabla \cdot \mathbf{v} \, d\mathbf{x} = 0 \end{aligned} \right. \quad (25a)$$

$$\text{for } k = 1, 2, \dots, N_G \left\{ \int_{\partial G_k} (\mathbf{u} \cdot \mathbf{n}_k - \mathbf{U}_k \cdot \mathbf{n}_k) \mu_{\partial G} \, d\ell = 0 \right. \quad (25b)$$

$$\left. \int_G \nabla \cdot \mathbf{u} \mu_G \, d\mathbf{x} = 0 \right. \quad (25c)$$

$$\forall \mathbf{v} \in H(\text{div}, \Omega), \mathbf{V}_k \in \mathbb{R}^2, \mu_{\partial G} \in H^{1/2}(\partial G), \mu_G \in H^1(G)$$

with μ_G and $\mu_{\partial G}$ test functions of $\lambda_{\partial G}$ et λ_G respectively.

2.3.3. Linearized continuity equation for the extended domain

Now, let us include Eq. (9b) into the system (25). We write the weak form of the divergence free constraint (20):

$$\int_G \nabla \cdot \mathbf{u} q \, dx = 0 \quad \forall q \in L^2(G) \quad (26)$$

Note that Eq. (26) is redundant with Eq. (25c). Consequently, we can directly extend Eq. (9b) to Ω because Eq. (25c) is enforced anyway. The final problem consists in finding $\mathbf{u} \in H(\text{div}, \Omega)$, $\mathbf{U}_k \in \mathbb{R}^2$, $p \in L^2(\Omega)$, $\lambda_{\partial G} \in H^{1/2}(\partial G)$, and $\lambda_G \in H^1(G)$ such as:

$$\left\{ \begin{array}{l} \int_{\Omega} \rho_0 \frac{\partial \mathbf{u}}{\partial t} \cdot \mathbf{v} \, dx - \int_{\Omega} p \nabla \cdot \mathbf{v} \, dx + \sum_k \left[(\rho - \rho_0) S_k \frac{d\mathbf{U}_k}{dt} \cdot \mathbf{V}_k - \mathbf{F}_k \cdot \mathbf{V}_k \right] \\ \quad + \sum_k \left[\int_{\partial G_k} \lambda_{\partial G} (\mathbf{v} \cdot \mathbf{n}_k - \mathbf{V}_k \cdot \mathbf{n}_k) \, d\ell \right] + \int_G \lambda_G \nabla \cdot \mathbf{v} \, dx = 0 \quad (27a) \\ \int_{\Omega} \frac{1}{\rho_0 c_0^2} \frac{\partial p}{\partial t} q \, dx + \int_{\Omega} \nabla \cdot \mathbf{u} q \, dx = 0 \quad (27b) \\ \text{for } k = 1, 2, \dots, N_G \left\{ \int_{\partial G_k} (\mathbf{u} \cdot \mathbf{n}_k - \mathbf{U}_k \cdot \mathbf{n}_k) \mu_{\partial G} \, d\ell = 0 \quad (27c) \right. \\ \left. \int_G \nabla \cdot \mathbf{u} \mu_G \, dx = 0 \quad (27d) \right. \\ \forall \mathbf{v} \in H(\text{div}, \Omega), \mathbf{V}_k \in \mathbb{R}^2, q \in L^2(\Omega), \mu_{\partial G} \in H^{1/2}(\partial G), \mu_G \in H^1(G) \end{array} \right.$$

Eq. (27) can be solved only if $\rho_0 \neq \rho$, otherwise the unknown disappears from Eq. (27a). A similar case occurs in [16] for Navier-Stokes equations but another fictitious domain formulation was found to deal with this specific issue in [23]. We do not treat the case where the density of the fluid ρ_0 is the same as the density of the grain ρ because it is not relevant in the case of our geophysical applications. Moreover, [23] does not refer to an explicit velocity of the grain \mathbf{U}_k which we need for the discrete algorithm we use.

3. Computational scheme

3.1. Finite elements

With the fictitious domain approach, two independent meshes have to be considered: one for the global domain Ω and one for the domain of grains G . A regular grid \mathcal{T}_{Ω_h} (see Fig. 2a) is used for the rectangular domain Ω to allow use of optimization techniques for the computation of the pressure and velocity fields p and \mathbf{u} . The second grid \mathcal{T}_{G_h} (Fig. 2b) refers to the domain of grains G : this grid may be unstructured but requires specific quadrature formula to perform the numerical integration on triangles. So we prefer to choose a pseudo-regular grid as in [24] to keep variational spaces simple.

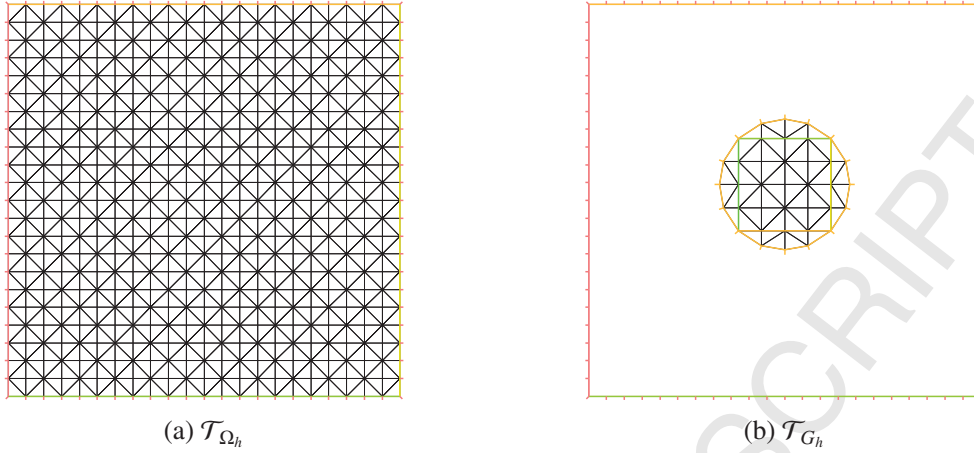


Figure 2: The regular grid \mathcal{T}_{Ω_h} (on the left) is the grid where the physical variables \mathbf{u} and p are computed and the unstructured grid \mathcal{T}_{G_h} (on the right) is the domain of the Lagrange multipliers.

Furthermore, \mathcal{T}_{G_h} is independent from the grid \mathcal{T}_{Ω_h} and can be shifted during the simulation. However, the size of the two meshes cannot be chosen independently; there is a compatibility condition that must be satisfied so that the fictitious domain method converges [10]. Concretely, we choose in our experiments a mesh ratio of $\kappa \approx 1.2$ which yields results in good agreement with analytic solutions.

We use the free software *FreeFEM++* [25] to generate meshes and solve the partial differential equations. In fact, *FreeFEM++* works in the same way as Matlab does, i.e. with its own high-level programming scripting language, close to the C language. So it is easy to implement both finite elements and the discrete element method governing the motion of grains. The full access to matrices also allows them to be modified to include constraints of the fictitious domain method.

In [18], we based our finite element approximation on the lowest order Raviart-Thomas element RT_0 [26] which is the natural choice to discretize the functional space $H(\text{div}; \Omega)$. Despite the validation of the particle velocities in [18], the examination of the acoustic fields pointed out serious issues with RT_0 element. Indeed, convergence issues were also revealed in [27] while using the fictitious domain method with Neumann boundary condition and the RT_0 element. We solve these problems in the present paper by opting for mixed methods using standard conforming finite elements [28]. Lagrangian finite elements are used to approximate the solutions: the piece-wise constant element P_{0_h} for the pressure space $L^2(\Omega)$ is defined as:

$$P_{0_h} = \{q_h \in L^2(\overline{\Omega_h}) \mid \forall K \in \mathcal{T}_{\Omega_h}, q_h|_K = \beta_K\} \quad (28)$$

with K a triangular finite element. The continuous piece-wise linear element P_{1_h} is used to discretize the velocity space $H(\text{div}; \Omega)$ in \mathcal{T}_{Ω_h} :

$$P_{1_h} = \{v_h \in C^0(\overline{\Omega_h}) \mid \forall K \in \mathcal{T}_{\Omega_h}, v_h|_K \in P_1\} \quad (29)$$

and also the Lagrange multipliers spaces $H^1(G)$ in \mathcal{T}_{G_h} and $H^{1/2}(\partial G)$ on $\mathcal{T}_{\partial G_h}$.

3.2. Finite-differences time-domain method

3.2.1. Operator splitting scheme

System (27) is too intricate to be solved directly using a standard finite difference scheme. It has to be separated into smaller subproblems using the Marchuk's first order operator splitting scheme [29]. Consider the problem :

$$\frac{\partial \varphi}{\partial t} + A(\varphi) = f \quad \text{and} \quad \varphi|_{t=0} = \varphi_0 \quad (30)$$

where $A = \sum_{\alpha=1}^N A_\alpha$, $A_\alpha \geq 0$, $N \geq 2$ and A is time-independent. The absolutely stable algorithm is, for $j = 0, 1, \dots, N$:

$$\begin{aligned} \frac{\varphi^{j+\frac{1}{N}} - \varphi^j}{\Delta t} + A_1(\varphi^{j+\frac{1}{N}}) &= f_1^{j+1} \\ &\vdots \\ \frac{\varphi^{j+1} - \varphi^{j+\frac{N-1}{N}}}{\Delta t} + A_N(\varphi^{j+1}) &= f_N^{j+1} \end{aligned} \quad (31)$$

with Δt the time step. To apply this algorithm, the system (27) is subdivided into two steps discussed in detail below:

1. propagate the acoustic wave in the fluid (*step 1a*); compute position, velocity and forces acting on the grains (*step 1b*),
2. enforce constraints applied on the grains (*step 2*).

We compute the acoustic velocity field and grain velocities at the same time because they are linked through the same velocity space, so they both correspond with step 1 of Marchuk's algorithm. However, resolutions of the acoustic wave equation and the equation of motion are totally independent inside step 1.

3.2.2. Step 1a: wave equation with semi-implicit Euler

Firstly, we solve the wave equation system by finding $\mathbf{u}_h \in P_{1h}^2$ and $p_h \in P_{0h}$ such as:

$$\left\{ \int_{\Omega} \frac{1}{\rho_0 c_0^2} \frac{\partial p_h}{\partial t} q_h \, d\mathbf{x} + \int_{\Omega} \nabla \cdot \mathbf{u}_h q_h \, d\mathbf{x} = 0 \right. \quad (32a)$$

$$\left. \int_{\Omega} \rho_0 \frac{\partial \mathbf{u}_h}{\partial t} \cdot \mathbf{v}_h \, d\mathbf{x} - \int_{\Omega} p_h \nabla \cdot \mathbf{v}_h \, d\mathbf{x} = 0 \right. \quad (32b)$$

$\forall \mathbf{v}_h \in P_{1h}^2$ and $q_h \in P_{0h}$. We can solve successively equations (32a) and (32b) using the following first order semi-implicit Euler scheme :

1. find $p_h^{n+\frac{1}{2}} \in P_{0h}$ such as:

$$\int_{\Omega} \frac{1}{\rho_0 c_0^2} \frac{p_h^{n+\frac{1}{2}} - p_h^n}{\Delta t} q_h \, d\mathbf{x} + \int_{\Omega} \nabla \cdot \mathbf{u}_h^n q_h \, d\mathbf{x} = 0 \quad \forall q_h \in P_{0h} \quad (33)$$

2. find $\mathbf{u}_h^{n+\frac{1}{2}}$ such as:

$$\int_{\Omega} \rho_0 \frac{\mathbf{u}_h^{n+\frac{1}{2}} - \mathbf{u}_h^n}{\Delta t} \cdot \mathbf{v}_h \, d\mathbf{x} - \int_{\Omega} p_h^{n+\frac{1}{2}} \nabla \cdot \mathbf{v}_h \, d\mathbf{x} = 0 \quad \forall \mathbf{v}_h \in P_{1h}^2 \quad (34)$$

with $t = \Delta t_{\min}$. In the semi-implicit Euler scheme, the minimal time step Δt_{\min} is related to the minimal spatial step h_{\min} by:

$$\Delta t_{\min} \leq \frac{\alpha}{c_0} h_{\min} \quad (35)$$

where α is a positive number.

3.2.3. Step 1b: equation of motion with Verlet algorithm

Independently to the computation of the wave equation (33) and (34), we can solve the part of the system corresponding to the equation of motion. Find $\mathbf{U}_k \in \mathbb{R}^2 \forall k = 1, 2, \dots, N_G$ such as:

$$(\rho - \rho_0) S_k \frac{d\mathbf{U}_k}{dt} \cdot \mathbf{V}_k - \mathbf{F}_k \cdot \mathbf{V}_k = 0 \quad \forall \mathbf{V}_k \in \mathbb{R}^2 \quad (36)$$

We use the Molecular Dynamics algorithm [5, 6] to compute forces, integrate the equation of motion for each grain and govern interactions between rigid grains. We choose to solve the equation of motion in three parts using the Verlet algorithm [30, 31].

1. First, position of the grain $\mathbf{X}_k^{n+\frac{1}{2}}$ is computed:

$$\mathbf{X}_k^{n+\frac{1}{2}} = \mathbf{X}_k^n + \Delta t \mathbf{U}_k^n + \frac{\Delta t}{2} \mathbf{A}_k^n \quad (37)$$

2. Secondly, all forces \mathbf{F} depending on the positions are computed:

$$\mathbf{A}_k^{n+\frac{1}{2}} = \frac{\mathbf{F}(\mathbf{X}_k^{n+\frac{1}{2}})}{(\rho - \rho_0) S_k} \quad (38)$$

3. Finally, the velocity is deduced from the acceleration values:

$$\mathbf{U}_k^{n+\frac{1}{2}} = \mathbf{U}_k^n + \frac{\Delta t}{2} (\mathbf{A}_k^{n+\frac{1}{2}} + \mathbf{A}_k^n) \quad (39)$$

3.2.4. Step 2: enforcement of constraints with conjugate gradient algorithm

In the second time step of Marchuk's operator splitting scheme, the jump condition of the acoustic wave equation is applied on the boundary ∂G and the rigid body motion constraint is applied inside the grain G . This leads to find $\mathbf{u}_h^{n+1} \in P_{1h}^2$, $\mathbf{U}_k^{n+1} \in \mathbb{R}^2$, $\lambda_{\partial G_h}^{n+1} \in P_{1h}$ and $\lambda_{G_h}^{n+1} \in P_{1h}$

such as:

$$\left\{ \begin{aligned} & \int_{\Omega} \rho_0 \frac{\mathbf{u}_h^{n+1} - \mathbf{u}_h^{n+\frac{1}{2}}}{\Delta t} \cdot \mathbf{v}_h \, d\mathbf{x} + \sum_k \left[(\rho - \rho_0) S_k \frac{\mathbf{U}_k^{n+1} - \mathbf{U}_k^{n+\frac{1}{2}}}{\Delta t} \cdot \mathbf{V}_k \right] \\ & + \sum_k \left[\int_{\partial G_k} \lambda_{\partial G_h}^{n+1} (\mathbf{v}_h \cdot \mathbf{n}_k - \mathbf{V}_k \cdot \mathbf{n}_k) \, d\ell \right] + \int_G \lambda_{G_h}^{n+1} (\nabla \cdot \mathbf{v}_h) \, d\mathbf{x} = 0 \quad (40a) \\ & N_G \text{ times } \left\{ \int_{\partial G_k} (\mathbf{u}_h^{n+1} \cdot \mathbf{n}_k - \mathbf{U}_k^{n+1} \cdot \mathbf{n}_k) \mu_{\partial G_h} \, d\ell = 0 \quad (40b) \right. \\ & \left. \int_G (\nabla \cdot \mathbf{u}_h^{n+1}) \mu_{G_h} \, d\mathbf{x} = 0 \quad (40c) \right. \end{aligned} \right.$$

$\forall \mathbf{v}_h \in P_{1_h}^2, \mathbf{V}_k \in \mathbb{R}^2, \mu_{\partial G_h} \in P_{1_h}$ and $\mu_{G_h} \in P_{1_h}$.

The discretized system (40) can also be represented as matrices:

$$\begin{pmatrix} \mathbf{A}_1 & \mathbf{0} & \mathbf{C}_1^T & \mathbf{C}_3^T \\ \mathbf{0} & \mathbf{A}_2 & \mathbf{C}_2^T & \mathbf{0} \\ \mathbf{C}_1 & \mathbf{C}_2 & \mathbf{0} & \mathbf{0} \\ \mathbf{C}_3 & \mathbf{0} & \mathbf{0} & \mathbf{0} \end{pmatrix} \begin{pmatrix} \mathbf{u}^{n+1} \\ \mathbf{U}^{n+1} \\ \lambda_{\partial G} \\ \lambda_G \end{pmatrix} = \begin{pmatrix} \mathbf{u}^{n+\frac{1}{2}} \\ \mathbf{U}^{n+\frac{1}{2}} \\ \mathbf{0} \\ \mathbf{0} \end{pmatrix} \quad (41)$$

To simplify the notation, we introduce block matrices \mathbf{A} , \mathbf{C} ; and vectors \mathbf{b} , \mathbf{d} , and λ :

$$\mathbf{A} = \begin{pmatrix} \mathbf{A}_1 & \mathbf{0} \\ \mathbf{0} & \mathbf{A}_2 \end{pmatrix} \quad \mathbf{C} = \begin{pmatrix} \mathbf{C}_1 & \mathbf{C}_2 \\ \mathbf{C}_3 & \mathbf{0} \end{pmatrix} \quad \mathbf{b} = \begin{pmatrix} \mathbf{u}^{n+1} \\ \mathbf{U}^{n+1} \end{pmatrix} \quad \mathbf{d} = \begin{pmatrix} \mathbf{u}^{n+\frac{1}{2}} \\ \mathbf{U}^{n+\frac{1}{2}} \end{pmatrix} \quad \lambda = \begin{pmatrix} \lambda_{\partial G} \\ \lambda_G \end{pmatrix} \quad (42)$$

and we rewrite system (41) as:

$$\begin{pmatrix} \mathbf{A} & \mathbf{C}^T \\ \mathbf{C} & \mathbf{0} \end{pmatrix} \begin{pmatrix} \mathbf{b} \\ \lambda \end{pmatrix} = \begin{pmatrix} \mathbf{d} \\ \mathbf{0} \end{pmatrix} \quad (43)$$

Such system can be solved using Uzawa's method for the conjugate gradient algorithm [32]. We initialize the algorithm with an initial approximation λ_0 and we construct an approximation of the solution \mathbf{b} for $i = 0$ until convergence by successively solving:

$$\mathbf{A} \mathbf{b}_{i+1} = \mathbf{d} - \mathbf{C}^T \lambda_i \quad (44)$$

and computing:

$$\lambda_{i+1} = \lambda_i + \beta \mathbf{C} \mathbf{b}_{i+1} \quad (45)$$

with β a scalar.

The optimal rate of convergence of the algorithm is given by [33]:

$$\beta = \frac{2}{\mu_1 + \mu_2} \quad (46)$$

with μ_1 and μ_2 the minimum and maximum eigenvalues of the Schur complement of sytem (43) $\mathbf{C} \mathbf{A}^{-1} \mathbf{C}^T$.

3.2.5. Velocity integration

Independently of Marchuk's algorithm and after solving the system (40b), we integrate the final velocity \mathbf{U}_k^{n+1} of the grains to get their next position. We simply integrate the velocity for the whole time step to retrieve updated position of grains:

$$\mathbf{X}_k^{n+1} = \mathbf{X}_k^n + \frac{\Delta t}{2} (\mathbf{U}_k^{n+1} + \mathbf{U}_k^n) \quad (47)$$

Then the mesh \mathcal{T}_{G_h} is updated with the new positions \mathbf{X}_k^{n+1} without modifying the regular mesh \mathcal{T}_{Ω_h} (Fig. 2).

4. Numerical experiments

In this part, we apply the method developed in sections 2 and 3 on three examples. On one hand, one movable grain is subject to an incident plane wave, and numerical results on dynamics and the acoustics are compared to analytic solutions. On the other hand two movable grains fixed by springs but without any incident plane wave illustrates energy transfers between fluid and grains. Finally we test a more realistic configuration of a random granular suspension with hundreds of grains to illustrate the possibilities of the model.

4.1. Movable grain in sound

To study the error compared to an analytic solution, we send a plane wave on a movable grain (Fig. 3). We first define a harmonic plane wave coming from the top (with $\theta_i = -\pi/2$ the incident angle) and defined as:

$$p_i(r, \theta, t) = A e^{i(kr \cos(\theta+\theta_i) - \omega t)} \quad (48)$$

with r the distance from the center of the grain and θ the observation angle. The pulsation ω and the wavenumber k are related to the frequency by $f = \frac{\omega}{2\pi} = \frac{k c_0}{2\pi}$. The diameter of the grain is $d = 2R = 1$ mm. At the beginning of the experiment, the center of the grain is located at coordinates (5; 4.5) mm. The size of the domain Ω is 10×10 mm and the size of PML layers on the top and bottom is $5 h_\Omega$. The source line is located at $y_{\text{src}} = 8.3$ mm and there are PML layers of thickness 0.4 mm on the top and on the bottom of the domain.

The wave velocity in the fluid medium is $c_0 = 1,500$ m/s. The density of the fluid medium is $\rho_0 = 1,000$ kg/m³ and the density of the material of grains is: $\rho = 2,500$ kg/m³. The frequency of the incident wave is $f = 1.5$ MHz which corresponds to a of $\lambda/d = 1$. The amplitude of the incident wave is $A = 1.5$ Pa in terms of pressure or $1 \mu\text{m/s}$ in terms of velocity.

We discretize the domain Ω with $N^2 = 120 \times 120$ nodes and so $h_\Omega = 1/12$ mm and the maximum mesh size of the fictitious domains satisfy $h_G \approx 1.2 \sqrt{2} h_\Omega$. We set parameter α of Eq. (35) related to the CFL condition of Euler semi-implicit scheme for the time discretization to $\alpha = 0.65/\sqrt{2}$. The duration of the simulation is $t_f = H/c_0$ with H the height of the domain Ω .

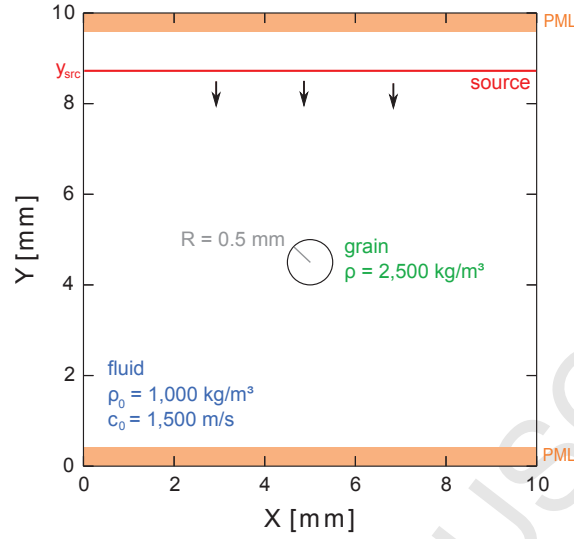


Figure 3: Scheme of the experiment with 1 grain

4.1.1. Pressure and velocity fields

The reference analytic solution for the pressure field scattered by a movable rigid disc can be written in cylindrical coordinates as [34]:

$$p_s(r, \theta) = \sum_{n=0}^{\infty} B_n H_n^{(1)}(kr) \cos(n(\theta - \theta_i)) \quad \forall r \geq R, 0 \leq \theta \leq 2\pi \quad (49)$$

with n an integer number and $H_n^{(1)}$ is the Hankel function of the first kind. The incident pressure field can also be rewritten as a sum of Bessel functions of the first kind J_n :

$$p_i(r, \theta) = A \left[J_0(kr) + 2 \sum_{n=1}^{\infty} i^n J_n(kr) \cos(n(\theta - \theta_i)) \right] \quad \forall r \geq R, 0 \leq \theta \leq 2\pi \quad (50)$$

B_n is a constant determined using Eqs. (49) and (50), and the boundary conditions applied on the grains defined in Eq. (3):

$$B_n = \begin{cases} -A \frac{J'_0(kR)}{H_0^{(1)\prime}(kR)} & \text{when } n = 0 \\ -2A i \frac{kR J'_1(kR) - \frac{\rho_0}{\rho} J_1(kR)}{kR H_1^{(1)\prime}(kR) - \frac{\rho_0}{\rho} H_1^{(1)}(kR)} & \text{when } n = 1 \\ -2A i^n \frac{J'_n(kR)}{H_n^{(1)\prime}(kR)} & \text{when } n \geq 2 \end{cases} \quad (51)$$

Then the total pressure field is the sum of the incident field p_i and the scattered field p_r :

$$p(r, \theta) = p_i(r, \theta) + p_r(r, \theta) \quad (52)$$

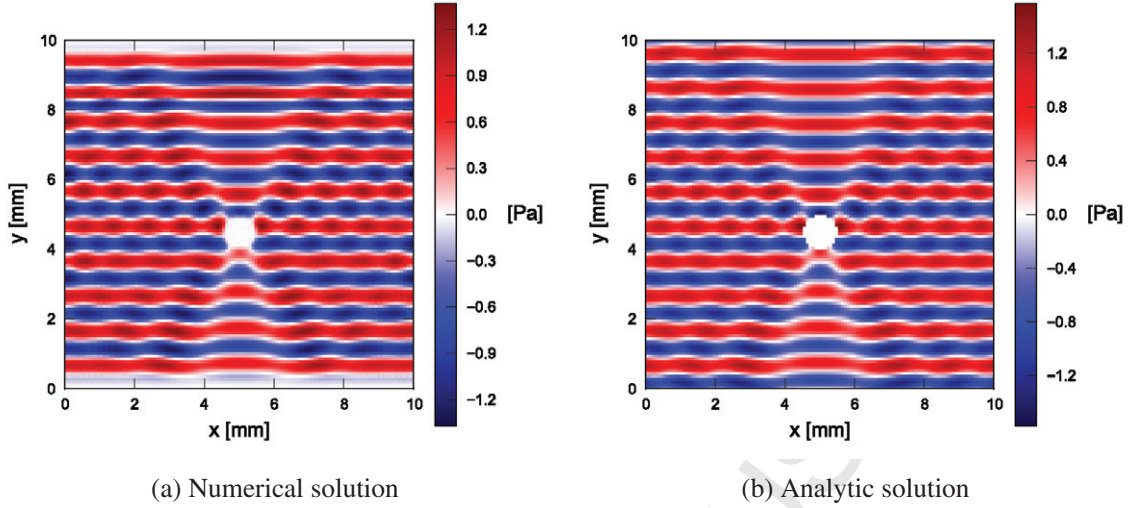


Figure 4: Numerical solution of the total pressure field computed using the fictitious domain method (4a) versus the analytic solution (4b) for $h_\Omega = 1/12$ mm.

Fig. 4a shows the total pressure field computed with the fictitious domain method and Fig. 4b shows the analytic solution computed using Eqs. (49) and (50). When comparing figures 4a and 4b, we observe that the numerical solution presents good agreements with the analytic solution.

Our model also provides the acoustic velocity field. The analytic solution of the total velocity field can be deduced from the solution of the pressure field Eq. (52):

$$\mathbf{u}(r, \theta) = \frac{-i}{\omega c_0} \nabla p(r, \theta) \quad (53)$$

Figure 5 represents numerical and analytic solutions of the total velocity field. We can see that the two velocity fields are quite similar. The difference at the top of the domain is a numerical artifact due to the source line that generates a plane wave in two opposite directions.

We define the relative error e_Φ for any field Φ during a period T as:

$$e_\Phi = \sup_{t_{\text{ref}} \leq t \leq t_{\text{ref}} + T} \left(\frac{\|\Phi_{\text{num}} - \Phi_{\text{an}}\|_{L^2}}{\|\Phi_{\text{an}}\|_{L^2}} \right) \quad (54)$$

with $t_{\text{ref}} = H/c_0$ the time for the wave to propagate through the entire medium. The relative error e_Φ is computed inside a square of size $[1.5; 8.5] \times [1; 8]$ mm to avoid PML and the effect of lateral periodic boundary conditions. Relative errors computed for fields p , u_x and u_y are reported in Table 1. The growth of the error on the acoustic fields is not optimal, revealing the weakness of Lagrangian finite elements when used in mixed methods [28]. The agreement of the numerical solution with the analytic solution (Figs. 5 and 4) shows nevertheless that the fictitious domain method converges with the element P_1 - P_0 on the contrary of the Raviart-Thomas element used in [18].

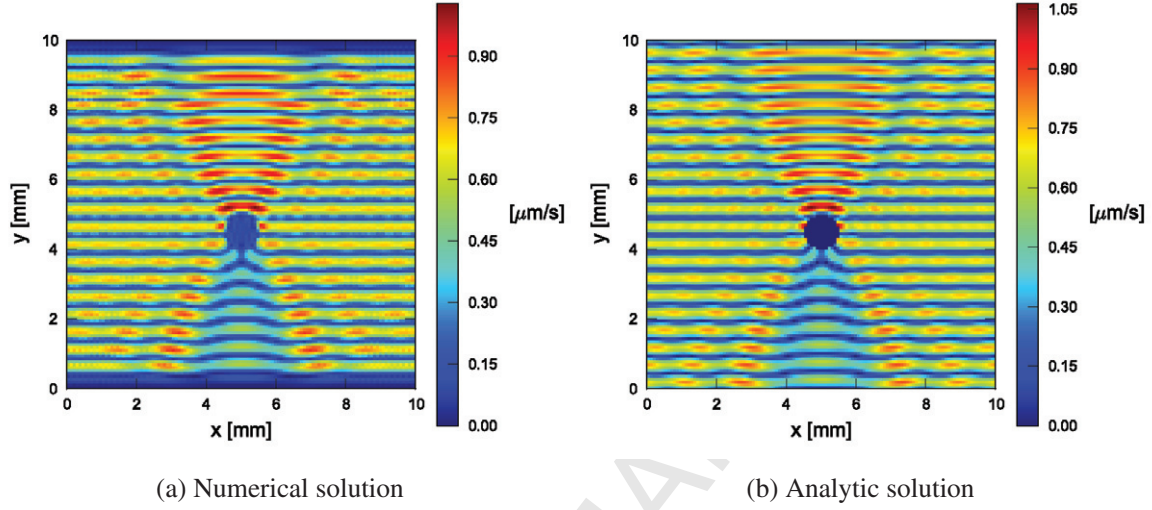


Figure 5: Numerical solution of the norm of the total velocity field computed using the fictitious domain method (5a) versus the analytic solution (5b) for $h_{\Omega} = 1/12$ mm.

Table 1: Relative errors computed for pressure and velocity fields for different discretizations

N^2	h_{Ω}	e_p	e_{u_x}	e_{u_y}
120^2	1/12 mm	1.44×10^{-1}	2.38×10^{-1}	1.47×10^{-1}
240^2	1/24 mm	9.19×10^{-2}	1.28×10^{-1}	9.01×10^{-2}
480^2	1/48 mm	8.00×10^{-2}	1.09×10^{-1}	7.93×10^{-2}

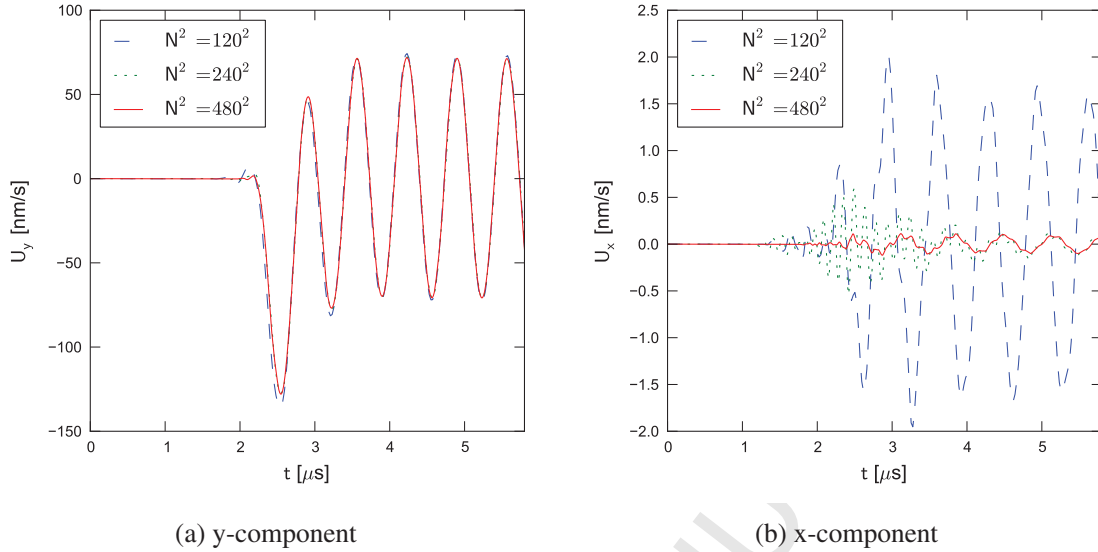


Figure 6: Velocity of the grain function of the time computed using the fictitious domain method for several discretizations.

4.1.2. Velocity of the grain

The main feature of the model is to take into account the dynamic of the grain submitted to an incident wave. We plot on Figure 6 the velocity of the grain as a function of the time for three discretizations at $t = 2.2 \mu\text{s}$. We observe on Fig. 6a that grains start to oscillate at the same frequency as the incident wave, when the wavefront reaches its location.

The x-component of the velocity of the grain can also be assimilated to an absolute error because it should be $U_x = 0$ according to the analytic solution. So we note on Fig. 6b that the decrease of maximal error is better for the velocity of the grain than for the norm of the velocity field. Indeed, the scale of the grain is larger than the one of the finite elements and the grain is therefore less sensitive to small perturbations of the pressure field.

4.2. Two movable grains fixed by springs

We perform a second experiment to show that the model can describe acoustic emissions directly coming from one grain subject to an external force \mathbf{F}_k . Most numerical methods in acoustics can not work without an incident wave. In this experiment, we link each grain with its own spring of stiffness $k_G = 100 \text{ GN/m}$ (to keep approximately the same frequency as in the previous example $f = \sqrt{(k/m)/(2\pi)}$), so that the external force \mathbf{F}_k from Eq. (2) p. 3 becomes:

$$\mathbf{F}_k = -k_G (Y_k - Y_{k_{\text{eq}}}) \mathbf{y} \quad (55)$$

with \mathbf{y} the unitary vector of the y-axis and $Y_{k_{\text{eq}}}$ the equilibrium position of the spring of the grain k . The bottom grain has an initial displacement from equilibrium $\Delta Y_0(t=0) = +1 \text{ pm}$ and the top grain is at its equilibrium position (see scheme Fig. 7a). Both are put in the middle of a domain of size $15 \times 17 \text{ mm}$ and at a distance of 1 mm of each other. We set PML on each side of the box

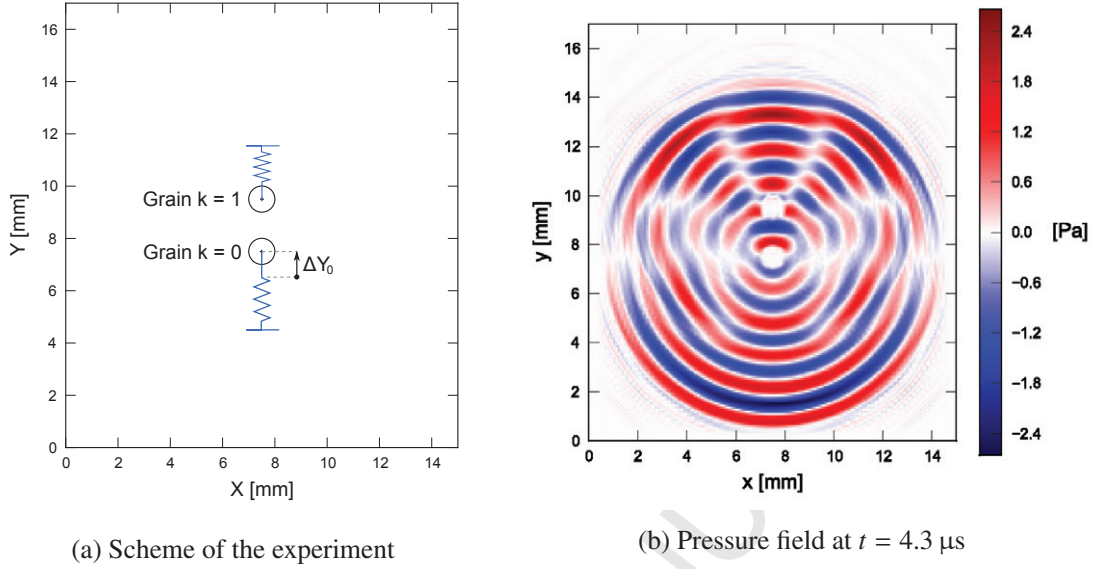


Figure 7: Numerical experiment of two movable grains fixed by springs. Fig. 7a shows a simplified representation of the experiment and Fig. 7b the pressure field at the final time $t = 4.3 \mu\text{s}$.

but we stop the simulation before the wavefront reaches the layer. Figure 7b shows the numerical pressure field for a discretization step $h_\Omega = 1/12 \text{ mm}$ at the final time $t = 4.3 \mu\text{s}$.

We examine now to the energy inside the system which is composed, according to system (27), on one hand of acoustic energy in Ω :

$$E_a = \int_{\Omega} \frac{1}{2\rho_0 c_0^2} p^2 \, d\mathbf{x} + \int_{\Omega} \frac{1}{2}\rho_0 \mathbf{u}^2 \, d\mathbf{x} \quad (56)$$

and on the other hand of the mechanical energy of each grain k :

$$E_{m_k} = \frac{1}{2} k_G (Y_k - Y_{k_{\text{eq}}})^2 + \frac{1}{2} (\rho - \rho_0) S_k \mathbf{U}_k^2 \quad (57)$$

Energies of the wave and the two grains are plotted in Figure 8. First we observe that the total energy in the system is well conserved considering the first order numerical scheme used for the time discretization. We observe that at $t = 0$, all the energy is in the grain 0 (in blue Fig. 8) in the form of mechanical potential energy due to the initial stretching of the spring. Then the grain 0 starts to oscillate and generates an acoustic field so its mechanical energy is partially converted to acoustic energy (in red Fig. 8). At $t = 1 \mu\text{s}$, the wavefront of the wave coming from the grain 0 reaches the other grain 1 and a part of the acoustic energy is converted to mechanical energy of grain 1 (in green Fig. 8). Then because the grain 1 is starting to oscillate, it is also radiating and gives back some mechanical energy in the form of acoustic energy.

As a comparison, we do the same experiment replacing water by air. Results reported in table 2 confirms that a numerical model able to link the wave equation and the equation of motion is essential to take in account transfers of energy through both water and grains. On the contrary, it is insignificant in the air.

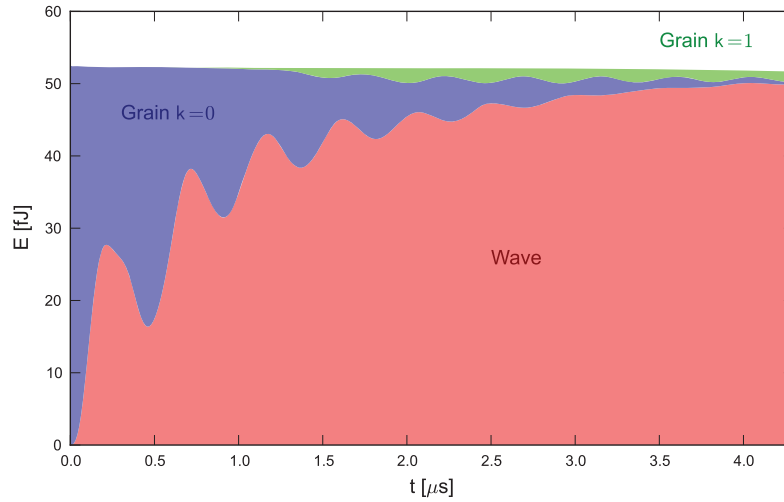


Figure 8: Evolution of the distribution of energy in the system containing two glass grains fixed by springs and surrounded by water

Table 2: Comparison of average energy distribution in water and in the air during the last period of oscillation

	water	air
c_0	1,500 m/s	340 m/s
ρ_0	1,000 kg/m ³	1.2 g/m ³
E_a	95.9 %	0.6 %
E_{m_0}	1.7 %	99.4 %
E_{m_1}	2.4 %	≈ 0 %

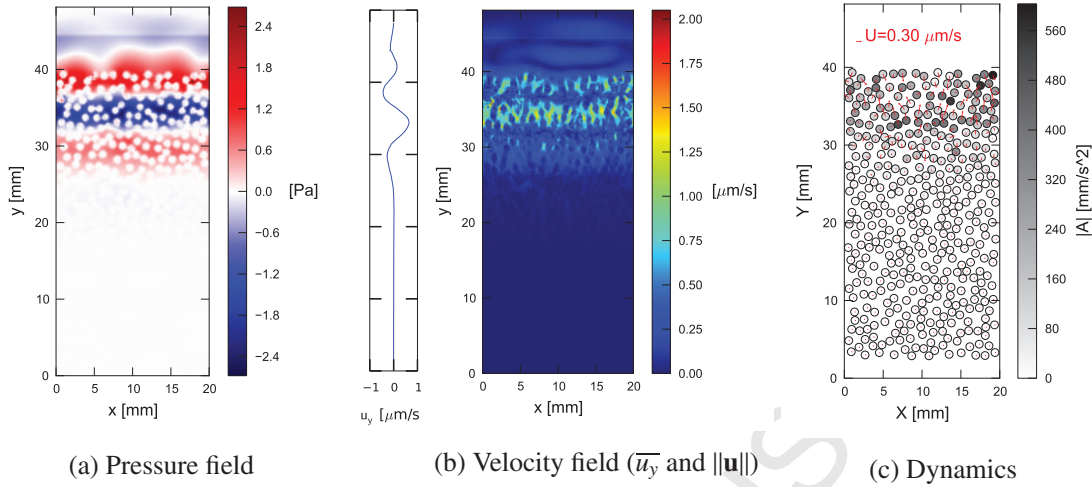


Figure 9: Propagation of a pulse through a granular suspension at $t = 20 \mu\text{s}$. Fig. (a) shows the acoustic pressure field, Fig. (b) the mean of the y-component and the norm of the velocity field and Fig. (c) positions, velocities (represented by red arrows) and acceleration (in grayscale) of each grain.

4.3. Acoustic pulse propagation through a granular suspension

The last experiment involves a random suspension of 400 movable grains subject to a unique pulse. We show that the model is able to work with many grains, contrary to the one developed in [18]. The source is on a horizontal line located at $y_{\text{src}} = 4.4 \text{ cm}$ and the pulse is the 4th derivative of a Gaussian with the central frequency $f_c = 150 \text{ kHz}$. We choose a pulse to follow easily the propagation of the wave through the medium. We consider a case where the characteristic wavelength $\lambda/d = 10$ because displacement of grains is maximum at $\lambda/d \gg 1$. The domain Ω is a rectangle 2 cm width and 4.8 cm height discretized by $N_x \times N_y = 108 \times 260$ and so $h_\Omega = 5/27 \text{ mm}$. The boundary conditions are the same as in section 4.1: PML on the top and on the bottom; and periodic boundary conditions on the left side and right sides.

Fig. 9 show snapshots of the pressure field (a), the velocity field (b) and positions, velocities and acceleration of each grain (c). The thin figure between the velocity field snapshot and the pressure field snapshot shows the mean value of the y-component of the velocity field and helps the reader to follow the propagation of the pulse. The variations of pressure (Fig. 9a) around the grains determine the value of the hydrodynamic force acting on them. Since the hydrodynamic force is the unique force, its value is proportional to the acceleration \mathbf{A} (in gray scale Fig. 9c).

Moreover, by observing red arrows in Fig. 9c, we can see that the wave sets in motion grains under its acoustic field. The result of the ratio between the amplitude of the velocity of one grain and the amplitude of the velocity field is provided by the following 2D analytic solution for low wavelength (inspired from the 3D version in [35]) :

$$\frac{\|\mathbf{U}\|}{\|\mathbf{u}\|} = \frac{2\rho_0}{\rho + \rho_0} \approx 0.57 \quad (58)$$

Comparison of Figs. 9b and 9c shows that numerical results are similar to the one predicted by the analytic solution.

Then, we can see Fig. 10 that the pulse propagates through the granular suspension from the top to the bottom. The mean value of the amplitude the velocity field Fig. 10b shows that the amplitude of the wave is decreasing as the energy of the wave is transmitted to the grains Fig. 10c. We also observe on Fig. 10a several other reflections after the wave pass. Thus, we can use solution (58) only at the beginning of the propagation when grains only subject to the incident wave not yet reflected waves from their neighbors.

5. Conclusions and discussion

Our results show that this fictitious domain method can couple the acoustic wave equation and the equation of motion for rigid grains. We show this using three numerical experiments. First, both acoustic fields and dynamics of grains computed using this model satisfy the analytical solution of a plane wave diffracted by a movable grain. In the second case, energy is transmitted between two grains and the fluid without loss of total energy. The last experiment shows that this method can also be expanded to hundreds of grains and used in the framework of acoustic experiments on granular suspensions.

The strength of this model is the ability of each grain to generate its own acoustic field when subject to an external force or due to an incident wave. As far as we know, there are no other acoustic model capable of coupling dynamics of rigid grains and waves. The rigidity of grains implies an infinite velocity inside the grains but still a finite velocity through the contacts network of a granular packing. In our knowledge, our model is the only one able to record acoustic emissions related to any forces acting on the grains of a granular medium.

Nevertheless interesting comparative studies could be done by observing changes in the reflected wave signal while changing parameters related to contact forces or materials of the grains. In the particular framework of compact granular media, interaction forces are defined according to linear or elastic models to simulate repulsion and friction between grains. So waves generated by grains are then directly related to the parameters of these models. Therefore we plan to use our model to study acoustic waves emitted by a granular medium during a gravitational destabilization.

References

- [1] Y. Le Gonidec, D. Gibert, Multiscale analysis of waves reflected by granular media: Acoustic experiments on glass beads and effective medium theories, *J. Geophys. Res. - Sol. Ea.* 112 (B5) (2007) B05103. doi:10.1029/2006JB004518.
- [2] V. Y. Zaitsev, P. Richard, R. Delannay, V. Tournat, V. E. Gusev, Pre-avalanche structural rearrangements in the bulk of granular medium: Experimental evidence, *EPL* 83 (6) (2008) 64003. doi:10.1209/0295-5075/83/64003.
- [3] J.-L. Thiot, Y. Le Gonidec, B. Kergosien, Acoustic emissions in granular structures under gravitational destabilization, in: B. B. J. Linde, J. Paczkowski, N. Ponikwicki (Eds.), *Acoustics of ordered and disordered granular structures*, Vol. 1433 of AIP Conference Proceedings, International Congress on Ultrasonics 2011, AIP, Gdańsk, Poland, 2012, pp. 143–146. doi:10.1063/1.3703157.
- [4] V. Tournat, V. Y. Zaitsev, V. E. Gusev, V. Nazarov, P. Béquin, B. Castagnède, Probing weak forces in granular media through nonlinear dynamic dilatancy: clapping contacts and polarization anisotropy, *Phys. Rev. Lett.* 92 (2004) 085502. doi:10.1103/PhysRevLett.92.085502.

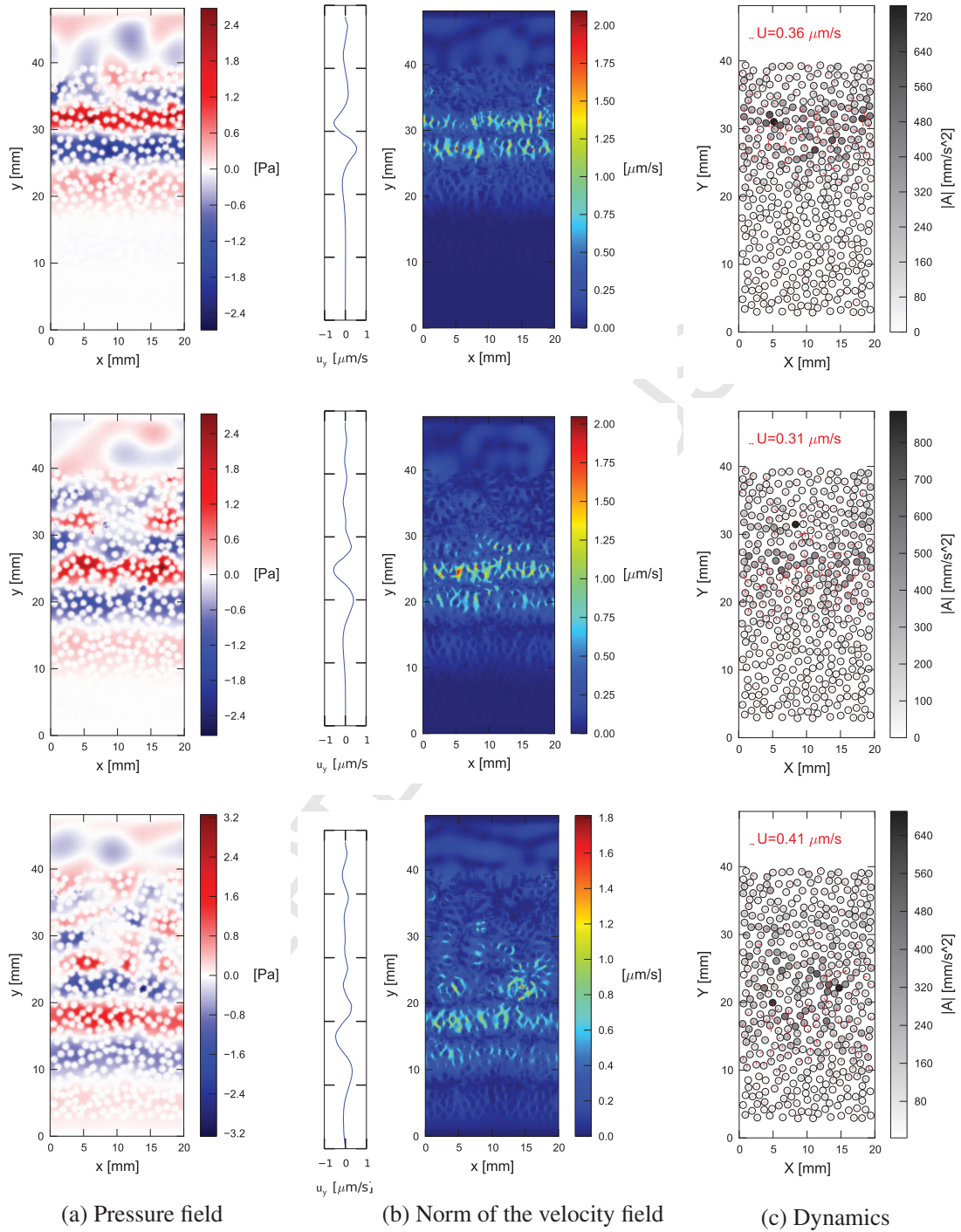


Figure 10: Propagation of a pulse through a granular suspension at $t = \{25; 30; 35\} \mu\text{s}$.

- [5] P. A. Cundall, O. D. L. Strack, A discrete numerical model for granular assemblies, *Géotechnique* 29 (1) (1979) 47–65. doi:10.1680/geot.1979.29.1.47.
- [6] S. McNamara, Méthode Dynamique Moléculaire, in: F. Radjai, F. Dubois (Eds.), *Modélisation numérique discrète de matériaux granulaires*, *Traité MIM - Mécanique et ingénierie des matériaux*, Hermès-Lavoisier, 2010, Ch. 1, pp. 25–48.
- [7] R. M. Alford, K. R. Kelly, D. M. Boore, Accuracy of finite-difference modeling of the acoustic wave equation, *Geophysics* 39 (6) (1974) 834–842.
- [8] D. Kosloff, D. Kessler, Seismic numerical modeling, in: Y. Desaubies, A. Tarantola, J. Zinn-Justin (Eds.), *Oceanographic and Geophysical Tomography*, Houches Summer Session, Elsevier Science, Les Houches, France, 1990, pp. 249–312.
- [9] O. C. Zienkiewicz, *The finite element method in engineering science*, McGraw-Hill, 1971.
- [10] I. Babuška, The finite element method with Lagrange multipliers, *Numer. Math.* 20 (3) (1973) 179–192. doi:10.1007/BF01436561.
- [11] R. Glowinski, T. Pan, J. Periaux, A Lagrange multiplier / fictitious domain method for the Dirichlet problem - generalization to some flow problems, *Jpn J. Ind. Appl. Math* 12 (1) (1995) 87–108. doi:10.1007/BF03167383.
- [12] E. Heikkola, Y. A. Kuznetsov, P. Neittaanmäki, J. Toivanen, Fictitious domain methods for the numerical solution of two-dimensional scattering problems, *J. Comput. Phys.* 145 (1) (1998) 89–109. doi:10.1006/jcph.1998.6014.
- [13] R. Glowinski, T. Pan, J. Periaux, Fictitious domain methods for incompressible viscous flow around moving rigid bodies, in: J. R. Whiteman (Ed.), *The Mathematics of Finite Elements and Applications*, 1996 MAFELAP Conference, Wiley, Brunel University, 1997.
- [14] L. Rhaouti, A. Chaigne, P. Joly, Time-domain modeling and numerical simulation of a kettledrum, *J. Acoust. Soc. Am.* 105 (6) (1999) 3545–3562. doi:10.1121/1.424679.
- [15] R. Glowinski, Y. Kuznetsov, On the solution of the Dirichlet problem for linear elliptic operators by a distributed Lagrange multiplier method, *CR Acad. Sci. I-Math.* 327 (7) (1998) 693–698. doi:10.1016/S0764-4442(99)80103-7.
- [16] R. Glowinski, T. Pan, T. Hesla, D. Joseph, A distributed Lagrange multiplier / fictitious domain method for particulate flows, *Int. J. Multiphase Flow* 25 (5) (1999) 755–794. doi:10.1016/S0301-9322(98)00048-2.
- [17] V. Bokil, R. Glowinski, An operator splitting scheme with a distributed Lagrange multiplier based fictitious domain method for wave propagation problems, *J. Comput. Phys.* 205 (1) (2005) 242–268. doi:10.1016/j.jcp.2004.10.040.
- [18] D. Imbert, S. McNamara, Fictitious domain method to model a movable rigid body in a sound wave, *J. Numer. Math.* 20 (3–4) (2012) 267–285. doi:10.1515/jnum-2012-0014.
- [19] J.-P. Berenger, A perfectly matched layer for the absorption of electromagnetic waves, *J. Comput. Phys.* 114 (2) (1994) 185–200. doi:10.1006/jcph.1994.1159.
- [20] W. C. Chew, W. H. Weedon, A 3D perfectly matched medium from modified Maxwell's equations with stretched coordinates, *Microw. Opt. Techn. Lett.* 7 (13) (1994) 599–604. doi:10.1002/mop.4650071304.
- [21] H. H. Hu, Direct simulation of flows of solid-liquid mixtures, *Int. J. Multiphase Flow* 22 (2) (1996) 335–352. doi:10.1016/0301-9322(95)00068-2.
- [22] B. Lombard, *Modélisation numérique de la propagation des ondes acoustiques et élastiques en présence d'interfaces*, Phd thesis, Université de la Méditerranée, 2002.
- [23] N. A. Patankar, P. Singh, D. D. Joseph, R. Glowinski, T.-W. Pan, A new formulation of the distributed Lagrange multiplier / fictitious domain method for particulate flow, *Int. J. Multiphase Flow* 26 (9) (2000) 1509–1524. doi:10.1016/S0301-9322(99)00100-7
- [24] R. Glowinski, T. Pan, J. Périaux, Distributed Lagrange multiplier methods for incompressible viscous flow around moving rigid bodies, *Comput. Methods Appl. Mech. Engrg.* 151 (1–2) (1998) 181–194. doi:10.1016/S0045-7825(97)00116-3.
- [25] F. Hecht, *FreeFem++*, Laboratoire Jacques-Louis Lions, Université Pierre et Marie Curie, Paris, 3rd Edition (2012).
URL <http://www.freefem.org/ff++/ftp/freefem++doc.pdf>
- [26] P. A. Raviart, J. M. Thomas, A mixed finite element method for 2-nd order elliptic problems, in: I. Galligani,

- E. Magenes (Eds.), *Mathematical Aspects of Finite Element Methods*, Vol. 606 of *Lecture Notes in Mathematics*, Springer, Rome, Italy, 1977, pp. 292–315. doi:10.1007/BFb0064470.
- [27] E. Bécache, J. Rodríguez, C. Tsogka, Convergence results of the fictitious domain method for a mixed formulation of the wave equation with a Neumann boundary condition, *ESAIM Math. Model. Num.* 43 (2) (2009) 377–398. doi:10.1051/m2an:2008047.
- [28] J. Li, T. Arbogast, Y. Huang, Mixed methods using standard conforming finite elements, *Comput. Methods Appl. Mech. Engrg.* 198 (5–8) (2009) 680–692. doi:10.1016/j.cma.2008.10.002.
- [29] G. I. Marchuk, *Splitting and alternating direction methods*, Vol. 1 of *Handbook of Numerical Analysis*, Elsevier, 1990. doi:10.1016/S1570-8659(05)80035-3.
- [30] L. Verlet, Computer "experiments" on classical fluids. I. Thermodynamical properties of Lennard-Jones molecules, *Phys. Rev.* 159 (1) (1967) 98–103. doi:10.1103/PhysRev.159.98.
- [31] W. C. Swope, H. C. Andersen, H. Berens, K. R. Wilson, A computer simulation method for the calculation of equilibrium constants for the formation of physical clusters of molecules: Application to small water clusters, *J. Chem. Phys.* 76 (1) (1982) 637–649. doi:10.1063/1.442716.
- [32] K. J. Arrow, L. Hurwicz, H. Uzawa (Eds.), *Studies in linear and non-linear programming*, Vol. 2 of *Stanford Mathematical Studies in the Social Sciences*, Stanford University Press, 1958.
- [33] H. C. Elman, G. H. Golub, Inexact and preconditioned Uzawa algorithms for saddle point problems, *SIAM J. Numer. Anal.* 31 (6) (1994) 1645–1661. doi:10.1137/0731085.
- [34] C. Potel, M. Bruneau, *Acoustique Générale - Équations différentielles et intégrales, solutions en milieux fluide et solide, applications*, Technosup, Ellipse, 2006.
- [35] H. Lamb, *Hydrodynamics*, sixième Edition, Dover publications, New York, 1945.